Global and Planetary Change 162 (2018) 163–174

Contents lists available at ScienceDirect

Global and Planetary Change

journal homepage: www.elsevier.com/locate/gloplacha

Interannual sea level variability in the Pearl River Estuary and its response to El Niño–Southern Oscillation

Linlin Wang[a], Qiang Li[a], Xian-zhong Mao[a,*], Hongsheng Bi[a,b], Peng Yin[a]

[a] Division of Ocean Science and Technology, Graduate School at Shenzhen, Tsinghua University, Shenzhen, PR China
[b] Chesapeake Biological Laboratory, University of Maryland Center for Environmental Science, Solomons, MD 20688, United States

ARTICLE INFO

Editor: Dr. Haywood Alan

Keywords:
Pearl River Estuary
ENSO
Interannual sea level variability
Sea level pressure
Wind-driven currents

ABSTRACT

The South China coast, especially the Pearl River Estuary (PRE) region, is prosperous and densely populated, but vulnerable to sea level changes. Sea level anomalies (SLA) during 1954–2012 from tide gauge station data and regional SLAs during 1993–2012 from satellite altimetry are analyzed and compare to the El Niño–Southern Oscillation (ENSO). Results show that sea level declines during El Niño events and rises during La Niña. Sea level in the PRE responds to ENSO with ~3–month lag. The ENSO can cause sea level in the PRE to fluctuate from −8.70 to 8.11 cm. Sea level cycles of 3 and 5 years are related to ENSO. The ENSO mechanism affecting sea level in the PRE was analyzed by identifying dominant regional and local forces. Weak/strong SLAs in most El Niño/La Niña events may be attributed to less/more seawater transport driven by anomalously weak/strong north winds and local anomalously high/low sea level pressure. Wind-driven coastal current is the predominant factor. It generated coastal seawater volume transport along a ~160 km wide cross section to decrease by 21.07% in a typical El Niño period (January 2010) and increase by 44.03% in a typical La Niña period (January 2011) as compared to an ENSO neutral situation (January 2013). Results of sea level rise and its potential mechanism provide insight for disaster protection during extreme El Niño/La Niña events.

1. Introduction

Coastal regions are often of economic importance, but are vulnerable to global sea level rise. The global sea level has risen at ~3.1 mm annually on average since the 1990s and continues to rise (Nerem et al., 2010; Church and White, 2011). However, global sea level changes are not at the same rate everywhere. Extensive studies have shown that greater rise rates of sea level occurred in the western tropical Pacific, southern oceans and eastern Indian Ocean in recent decades (Li et al., 2002; Cazenave and Nerem, 2004; Chowdhury et al., 2010; Tseng et al., 2010). At regional scale, the sea level rise rate in the South China Sea (SCS) is substantially higher than the global mean rate (Cheng and Qi, 2007; Fang et al., 2006). Locally, coastal areas of South China are also experiencing a faster rise rate than the global mean (Peng et al., 2013; Wang et al., 2016).

As the global temperature changes, so does the sea level. Sea level is often considered an effective indicator of climate change. Thermal expansion from global warming, water input from glaciers and ice sheets have changed sea level on various time scales (Cheng et al., 2008; Rahmstorf, 2007). Recent studies found that El Niño and La Niña events have strong impacts on sea level interannual variation (Llovel et al., 2011; Cazenave et al., 2012; Fasullo et al., 2013). Sea levels at low latitudes, i.e., tropical and subtropical, are more responsive to ENSO than at mid–high latitudes (Soumya et al., 2015; Yuan et al., 2009). Although ENSO has major impacts on the sea level in low-latitude regions, i.e., causing it to fluctuate, it has not altered the rising trend (Cheng et al., 2016). After removing interannual variability caused by ENSO, the global mean sea level in recent decades showed a continuous rapid rise rate of 3.3 ± 0.4 mm per year (Cazenave et al., 2014). Furthermore, spatial variations in extreme positive sea level anomalies over the past 20 years were closely associated with regional modes such as ENSO (Woodworth and Menendez, 2015).

In the western Pacific Ocean, interannual sea surface height (SSH) oscillations have been associated with ENSO (Chang et al., 2013; Zhuang et al., 2013). The SCS is a semi-closed sea exchanging water with the adjacent East China Sea, Indian Ocean and western Pacific Ocean (Fig. 1). In the SCS, ENSO affects sea surface temperature (SST), the monsoon, precipitation, and tropical cyclones (Nan et al., 2014; Wang et al., 2012; Chang et al., 2008; Q. Zhang et al., 2015; R. Zhang et al., 2015). ENSO also influences interannual sea level variation in the SCS at different spatial and temporal scales through various processes such as water transport, anomalous Ekman pumping, and anomalous

* Corresponding author.
E-mail address: maoxz@sz.tsinghua.edu.cn (X.-z. Mao).

https://doi.org/10.1016/j.gloplacha.2018.01.007
Received 14 September 2017; Received in revised form 6 January 2018; Accepted 8 January 2018
Available online 12 January 2018
0921-8181/

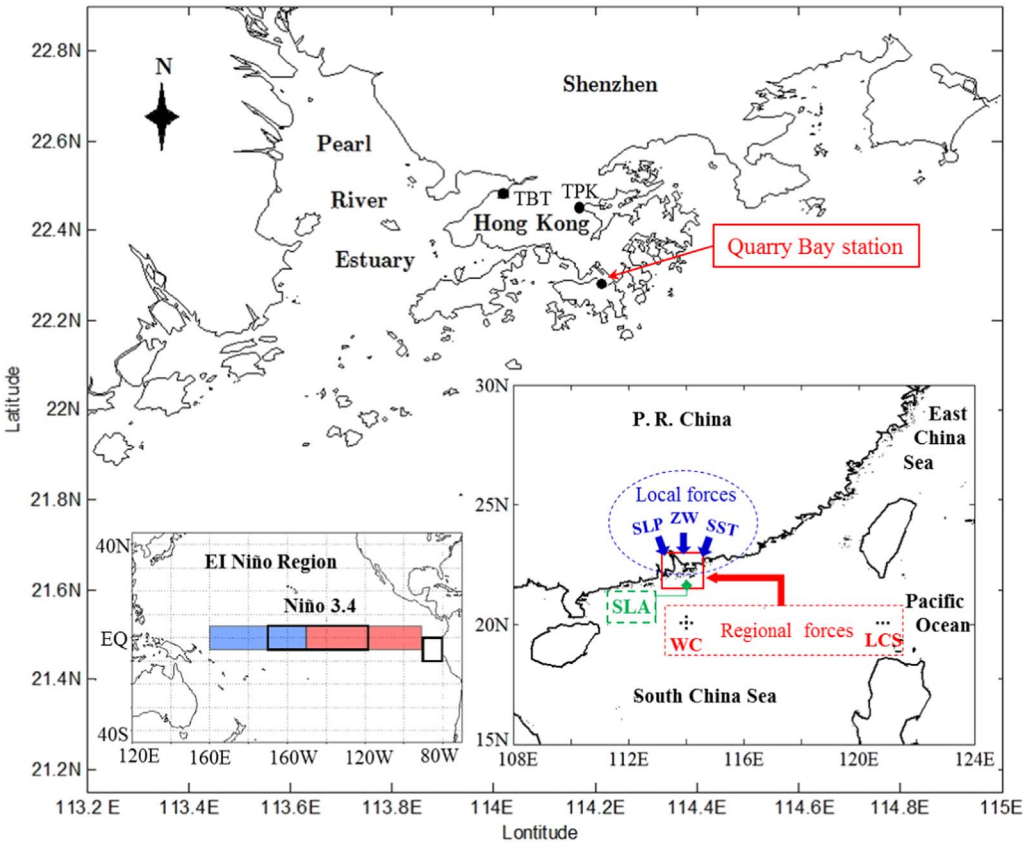

Fig. 1. Study area and locations of tide gauge stations in the PRE, representative regional SLA (green color), El Niño 3.4 region, and regional factors of Luzon Strait Current (LSC) and westward current (WC). Also shown are local forces of sea level pressure (SLP), zonal wind (ZW) and sea surface temperature (SST). (For interpretation of the references to color in this figure legend, the reader is referred to the web version of this article.)

SST (Chen et al., 2014; Han and Huang, 2009; Liu et al., 2011; Liu et al., 2015; Peng et al., 2013; Rong et al., 2007). Furthermore, ENSO may affect sea level maxima by modulating the number of tropical cyclones reaching China's coasts (Feng and Tsimplis, 2014).

The Pearl River Delta meets the northern SCS, with ~60 million people in the nine largest cities of the PRE region. This area is strongly affected by sea level rise (Shi et al., 2008; R. Huang et al., 2004; Z. Huang et al., 2004). The latest report from the China Oceanic Information Network estimates that the sea level at South China coasts will rise 75–165 mm in the next 30 years (http://www.coi.gov.cn). This will increase the risk of seawater intrusion (Yuan et al., 2015), with more sediment accumulation (Zhang and Mao, 2015; Wu et al., 2014) and coastal inundation (R. Huang et al., 2004; Z. Huang et al., 2004). This will in turn threaten freshwater supplies and human lives. In this region, sea level interannual variation is also affected by ENSO. For example, Ding et al. (2001a, b) found that sea level interannual variability in Hong Kong waters within the PRE was related to ENSO. However, the potential mechanism by which ENSO affects PRE sea level variation remains unclear and the impacts have not been quantified. The strong El Niño in 1997–1998 may have caused 32 million USD losses to Hong Kong fisheries because of anomalously warm seawater (Yin et al., 1999). Because the South China coast, especially the PRE, is economically important and densely populated, ENSO impacts should be quantified and related mechanisms investigated to provide insights for disaster prevention.

The overall objectives of the present study were to 1) quantify interannual variation of the PRE sea level, 2) examine how ENSO affects PRE sea level variability, specifically amplitude and periodicity, and 3) investigate potential drivers at multi-decadal scales and various spatial scales (including large, regional, and local). For prediction purposes, we also developed empirical models to quantify the relationship between sea level interannual variation in the PRE and ENSO.

2. Data and methods

2.1. Study area and data collection

Water level data from three tide gauge stations in Hong Kong waters of PRE were used to analyze sea level variation (Fig. 1). The Quarry Bay station is registered in the core network of the Global Sea Level Observing System, and its observed sea level data are often used to study long-term sea level changes (Ding et al., 2001a, b; Zhang and Ge, 2013). Two other stations, Tai Po Kau and Tsim Bei Tsui, are also within Hong Kong waters. However, only the Quarry Bay station has the longest and the most complete record of sea level and temperature data. Furthermore, that station is located off the mouth of the river and the effect of surface runoff is relatively weak. In a previous study, we found that water level data from the three stations were correlated, with correlations of 0.61–0.96. Moreover, the mean local SLA estimated from the three stations is correlated with offshore SLA, with a correlation coefficient of 0.73 (Wang et al., 2016). Therefore, the Quarry Bay station was selected for time series analysis. Regional SLAs from satellite altimetry for a broader region (19.5°–23.5°N and 111°–117.5°E) were downloaded from AVISO (http://www.aviso.altimetry.fr/) to analyze the relationship between regional SLA and ENSO.

The tide gauge data was provided by Hong Kong Observatory (HKO) and corrected for subsidence based on prior studies (Ding et al., 2001a, b). For hourly water level data, a 40-h lowess filter was applied to remove the tide-related component. Then, inverted barometer correction was done using sea level pressure (SLP) from the National Centers for Environmental Prediction (NCEP) (http://www.ncep.noaa.gov/) (Bi et al., 2011). The monthly water level was calculated after removing its linear trend. Finally, a 7-month moving average SLA was obtained to analyze sea level variations. The Butterworth filter with a band pass of 2 and 7 years was used to obtain the component of sea level variation related to ENSO.

The Southern Oscillation Index (SOI) and the Oceanic Niño Index

(ONI) were downloaded (http://www.ncdc.noaa.gov) to analyze potential ENSO impacts. The SOI reflects atmospheric anomalies between the eastern and western tropical Pacific, and the ONI represents the sea surface temperature anomaly (SSTA) in the Niño 3.4 region.

ENSO events are often characterized by temperature anomalies in the tropical Pacific, but can affect global temperature, atmosphere pressure, and weather patterns. Further, El Niño and La Niña events reflect large-scale atmosphere pressure fluctuations between the western and eastern tropical Pacific through the Walker circulation (Webster and Yang, 1992). Therefore, the SST and SLP in the PRE are likely affected by ENSO. Studies have shown that sea level interannual variability is related to ENSO in many low-latitude areas through wind-driven currents and seawater transport (Rong et al., 2007; Yuan et al., 2009). Since southern China is within the trade wind cell, local sea level may also be affected by trade winds and the equatorial ocean current. Luca et al. (2004) found that the Luzon Strait Current (LSC) can reach the interior SCS. Therefore, local wind and the LSC were analyzed to identify potential mechanisms of ENSO effects on SLA in the PRE.

SST data of 1975–2012 in the Hong Kong waters were provided by the HKO. SSTAs were calculated by removing 38-year monthly mean SST values. Monthly zonal wind and SLP data from 1954 to 2012 were downloaded from the NCEP (http://www.ncep.noaa.gov/). Zonal wind anomalies (ZWA) and SLP anomalies (SLPA) were calculated by removing 59-year monthly means of zonal wind and SLP, respectively. Twenty-year (1993–2012) geostrophic current velocities in the middle of the Luzon Strait were downloaded from AVISO (http://www.aviso.oceanobs.com) to examine the impacts of regional seawater movements on local sea level. Mean velocities were calculated by averaging the geostrophic current velocities at 20.125°N from 120.25°–121°E. LSC anomalies (LSCAs) were calculated by removing 20-year monthly mean LSC values. The westward current at ~20°N and ~114°E in the open sea about 65 km off the PRE was further analyzed to detect the effect of regional current (Fig. 1). Geostrophic current velocities for that current were calculated from a defined path starting from 20.125°N, 113.875°E to 20.375°N, 114.125°E (Fig. 1). Westward current anomalies (WCAs) were then calculated by removing the 20-year monthly mean westward current values.

2.2. Potential relationship between ENSO and sea level variation

To examine the relationship between ENSO and sea level variation, cross-correlation analysis was used to detect their correlations. For two time series $x(t)$ and $y(t)$ with length N, where $t = 1, 2 \ldots N$, the cross-correlation $r(\tau)$ at delay τ can be defined as (Ding et al., 2001b)

$$r(\tau) = \frac{\sigma_{xy}(\tau)}{\sqrt{\sigma_{xx}\sigma_{yy}}}, \quad (1)$$

where $\sigma_{xy}(\tau)$ is the lag τ cross-covariance between $x(t)$ and $y(t)$. σ_{xx} and σ_{yy} are the variances of $x(t)$ and $y(t)$, respectively.

2.3. Impacts of ENSO on frequency and magnitude of local sea level variation

Empirical mode decomposition (EMD) was used to identify the dominant amplitude and frequency in the sea level time series data $x(t)$. This method adaptively decomposes an input series into several intrinsic mode functions (IMF) having equal numbers of zero-crossing and extrema (or numbers differing at most by one). Envelopes of $e_{\min}(t)$ and $e_{\max}(t)$ are estimated from interpolation between local minima and maxima, respectively (Huang et al., 2003). The EMD procedure can ascertain the dominant modes (rapid oscillating components) in the series $x(t)$ and then iteratively subtract the less dominant modes (slowly oscillating components) that are local mean values in the series, $(e_{\min}(t) + e_{\max}(t)) / 2$. This procedure is terminated if all the dominant modes are identified. The local mean IMF value extracted is zero. The detailed procedure can be expressed as

$$x(t) = \sum_{j=1}^{M} d_j(t) + r(t), \quad (2)$$

where $r(t)$ is a monotonic function and reflects the trend of the series $x(t)$. $\{d_j(t)\}_{j=1}^{M}$ denotes M IMFs within the series. To minimize problems of pseudo-IMF signals and mode confusion, the mirrorizing extension method that adds extrema using mirror symmetry was applied to restrain end effects (Rilling et al., 2003).

2.4. Potential factors reflecting ENSO impacts

Potential factors were divided into regional and local levels based on their spatial scales. Regional drivers include the LSC and WC, which were mainly used to detect oceanic current anomalies caused by westerly trade winds in ENSO events. Local factors include sea level pressure, wind and sea surface temperature, which reflects local climate change caused by ENSO. The Butterworth filter with a band pass of 2 year and 7 year were used to obtain the components of these factors related to ENSO. Cross-correlation was conducted to detect their potential relationships with ENSO. Examining the impacts of regional and local factors may provide insight into the mechanism as to how ENSO events impact sea level in the PRE.

2.5. Impacts of ENSO in typical years using HYCOM

The Hybrid Coordinate Ocean Model (HYCOM) and Navy Coupled Ocean Data Assimilation global 1/12° analysis data (http://hycom.org/hycom) were used to study the impacts of 2-D SST and ocean currents on regional SSH. Surface downward northward wind stress data from NCEP Climate Forecast System Reanalysis and NCEP Climate Forecast System Version 2 (http://hycom.org/dataserver) were used to analyze regional wind impacts. SLP data with 0.125° × 0.125° resolution was downloaded from European Center for Medium-Range Weather Forecasts (ECMWF) (www.ecmwf.int/datasets) to study the impacts of regional air pressure during ENSO.

The El Niño (2009–2010) and La Niña (2010–2011) events and an El Niño neutral situation (2013) were studied using HYCOM data. Monthly mean SSH, SST, ocean current, SLP and wind stress in January 2010, 2011 and 2013 were analyzed to investigate ENSO impacts. These study periods avoided the effects of anomalous typhoons and floods. Upon considering ENSO strength and the delayed response of SSH, using SSH, SST, SLP and ocean current data from the El Niño neutral period (January 2013) as benchmarks, SLA, SSTA, SLPA and current anomalies in the El Niño and La Niña periods were calculated by subtracting the benchmarks.

3. Results

3.1. Relationship between SLA and ENSO

Sea level declined in 1954–1989 followed by a rapid rise in 1990–2001 (Fig. 2a and b). In recent years, sea level declined until 2009 and increased afterward. Small SOIs were frequent during the El Niño events, and the opposite occurred during the La Niña events (Fig. 2c). There are 18 years with El Niño events (1958, 1964, 1966, 1969, 1970, 1973, 1977, 1978, 1983, 1987, 1988, 1992, 1995, 1998, 2003, 2005, 2007 and 2010) and 18 years with La Niña events (1955, 1956, 1957, 1965, 1968, 1971, 1972, 1974, 1975, 1976, 1985, 1989, 1996, 1999, 2000, 2001, 2008 and 2011) over the period of 1954–2012. El Niño or La Niña event lasting for two or three consecutive years is considered as an ENSO event and total 15 El Niño events and 11 La Niña events were analyzed in Fig. 2. It can be found that although sea level changed significantly, relatively low/high sea levels were frequent in most El Niño/La Niña years (Fig. 2b) and Only 7

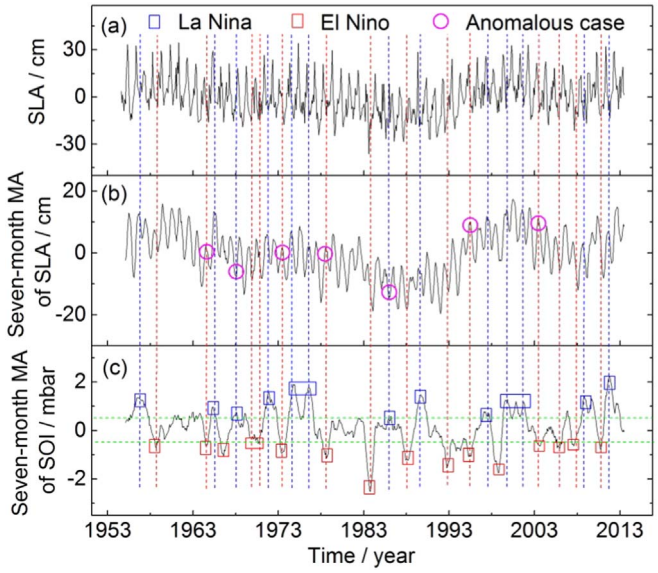

Fig. 2. Monthly average SLA (a), seven-month moving average (MA) of SLA (b), seven-month MA of Southern Oscillation Index (SOI) (c). Red and blue dashed vertical lines indicate El Niño and La Niña events; green horizontal lines indicate anomalously large fluctuations of SOI. (For interpretation of the references to color in this figure legend, the reader is referred to the web version of this article.)

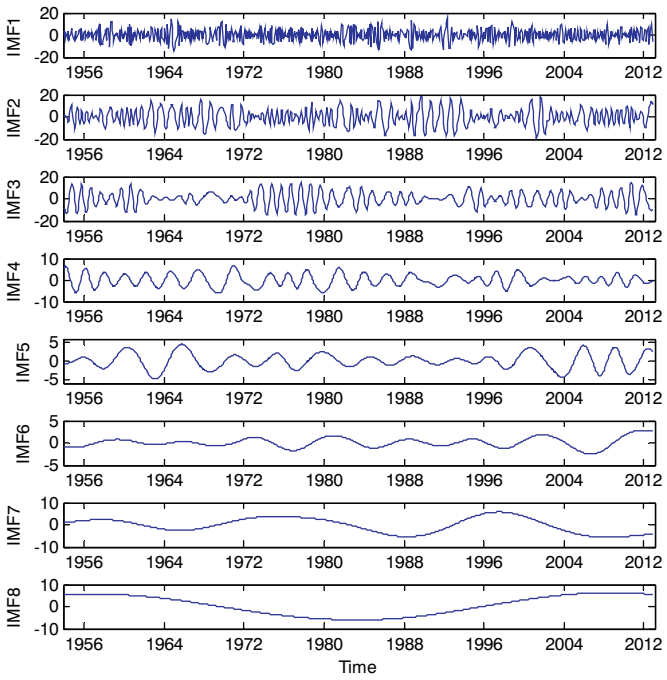

Fig. 4. Intrinsic mode function (IMF) signals of SLA in the PRE.

of the total 26 ENSO events had the reverse high/low sea levels in El Niño/La Niña events. Based on the maxima and minima distributions of SLAs over the past 59 years (Fig. 2b), there were three SLA maxima during three strong La Niña episodes in 1965, 1974–1976 and 1999–2001. Four SLA minima occurred during four strong El Niño episodes, e.g., 1983, 1987–1988, 2007 and 2010.

Based on the 7-month moving average of SLA and SOI over 1954–2012, the maximum correlation between SOI and SLA was 0.29 (exceeding the 95% lower and upper confidence thresholds shown in Fig. 3a) when SLA lagged by three months. To examine large-scale sea level changes relative to ENSO indices, a 2-D correlation map of the SOI and SLA from satellite altimetry for a broader region (19.5°–23.5°N and 111°–117.5°E) over 1993–2012 suggested correlations of 0.05–0.3, with larger values in South China coastal waters and the interior SCS (Fig. 3b). For the same period of 1993–2012, the maximum correlation of SOI and local SLA from tide gauge station was ~0.36 when local SLA lagged by three months. Overall correlation of SLA and SOI was ~0.3 and was greater at short timescales. The three-month lag of local SLA indicates that it took three months for the tropical ENSO to affect sea level in the PRE.

Eight IMF signals were identified from the time series of local SLA (Fig. 4). The periods of these signals ranged from seasonal (0.33 and 0.50 year), annual (1.01 year), interannual (3.56, 5.02 and 7.12 year) to decadal timescales (19.26 and 42.67 year). Potential mode confusion was small and only the 1.01-year period occurred in both IMF2 and IMF3. The periods of interannual variation, 3.56-year for IMF4 and 5.02-year for IMF5, were within the El Niño/La Niña cycle of 2–7 years. A new IMF4.5, the sum of IMF4 and IMF5, was created to represent the signal of sea level response to ENSO. The 7-month moving averages of IMF4.5 and SOI are shown in Fig. 5a. The two strongest periods of IMF4.5 were still ~3 (3.42) and ~5 (5.68) years. The strongest correlation between IMF4.5 and SOI was 0.3773 with 2–month lag (or 0.3735 with 3–month lag) of IMF4.5, indicating a 2–3 month delay of sea level. The 2–3 month lag of IMF4.5 was similar to the 3-month lag of overall SLA to ENSO but with stronger correlation (~0.38) with SOI,

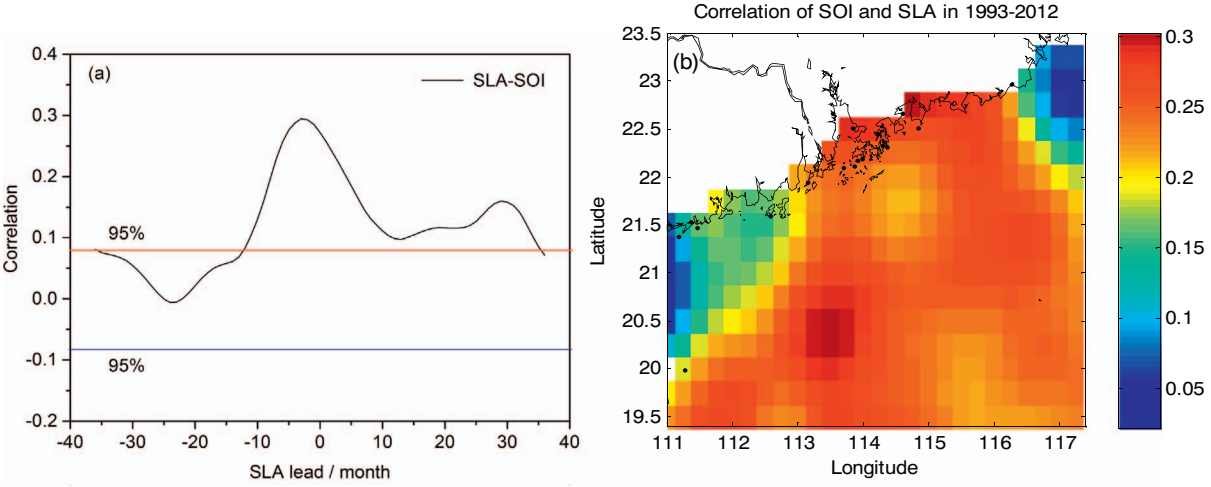

Fig. 3. Cross-correlations of local SLA with Southern Oscillation Index (SOI) over 1954–2012 (a) and 2-D correlations of regional SLAs from satellite altimetry with SOI over 1993–2012 (b).

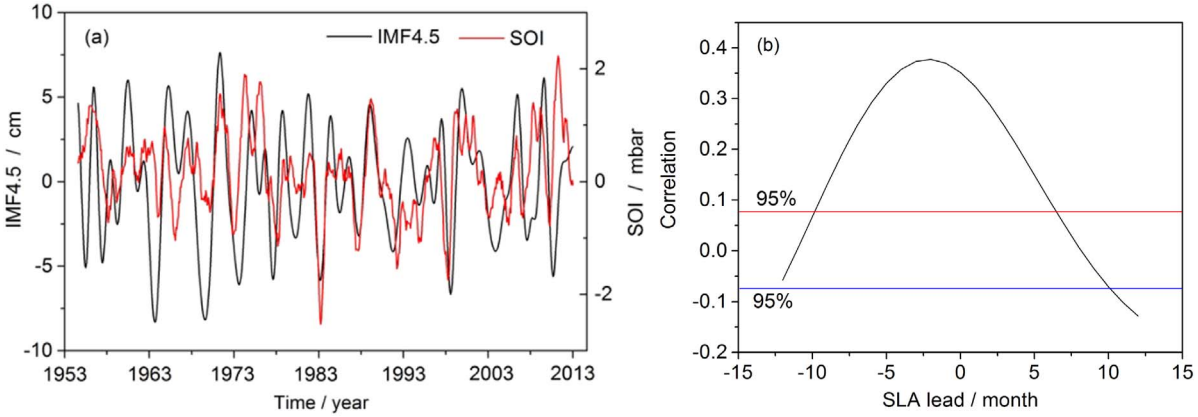

Fig. 5. Variations of seven-month moving average intrinsic mode function 4.5 (IMF4.5) and Southern Oscillation Index (SOI) (a) and their cross-correlation (b).

suggesting that the IMF4.5 signal effectively reflected the impacts of ENSO. Fluctuation of IMF4.5 was from −8.70 to 8.11 cm, which also indicates that the magnitude of ENSO affecting local SLA in the PRE was within 10 cm.

Fig. 6(a) shows the changes of IMF4.5 signal (periods of ~3 and ~5 years) and filter SLA (periods of 2–7 years) using the 2–7 years' band pass filter. The fluctuation of filter SLA was −6.96–6.38 cm, which was also within the magnitude of 10 cm. Although the fluctuation of filter SLA was a little smaller than that of IMF4.5, these two signals showed similar changes and their maximum correlation was ~0.79 with no time lag (Fig. 6c). The changes of filter SLA and SOI were also similar at most large and small SOI situations (Fig. 6b) and their maximum correlation was ~0.49 when filter SLA had 3-month lag (Fig. 6d). The similar changes and relatively high correlations of filter SLA with IMF4.5 and SOI indicates that the filter SLA was a sea level signal reflecting the effect of ENSO.

3.2. Impacts of regional and local factors on SLA

The changes of SOI, regional factors of LSCA and WCA, local factors of SSTA, SLPA and ZWA were given in Fig. 7 to detect whether ENSO could affect these factors. A negative LSCA indicates the westward water movement anomaly, i.e., seawater flowing into the SCS (Fig. 7a). Larger negative current anomalies indicated more surface seawater flowing into the SCS through the Luzon Strait. A negative WCA represents westward current anomalies (Fig. 7b). Preliminary analysis suggested that the SOI and SLA had stronger response to the zonal wind rather than the meridional wind. Therefore, we only analyzed the ZWA (Fig. 7e).

For these factors, the positive LSCA, WCA, SLPA and ZWA and negative SSTA, i.e., less seawater flowing into the SCS and the PRE, high SLP, weak north wind and low SST, could produce the weak SLAs in the PRE during El Niño events, and the opposite situations for La Niña events. The situations of LSCA (|LSCA| > 0.05 m/s), WCA (|WCA| > 0.03 m/s), SSTA (|SSTA| > 0.05 °C), SLPA (|SLPA| > 0.05 mbar) and ZWA (|ZWA| > 0.05 m/s) were regarded as anomalously large fluctuations and masked in green dash lines in Fig. 7.

Over 1993–2012, most El Niño (3 of 5 events)/La Niña (3 of 5 events) happened with strong negative/positive LSCA (Fig. 7a), indicating that more/less surface seawater flowing into the SCS. The discrepancy of more/less seawater flowing into the SCS and low/high SLA in the PRE suggests that LSCA may not be a key factor affecting sea level in the PRE in most El Niño/La Niña events. In Fig. 7(b), the strong positive/negative WCA, i.e., seawater flowing off/into the PRE happened in most El Niño events (4 of 5 events)/La Niña events (3 of 5 events), which would lead to the low/high SLAs after seawater divergence/accumulation. From Fig. 7(c), high/low SSTA happened in most El Niño (6 of 10 events)/La Niña events (6 of 7 events), which indicates that SSTA was not a factor causing the low/high SLAs in most El Niño/La Niña events. On the contrary, SSTA may play the role in modulating the falling/rising SLAs in most El Niño/La Niña events through seawater thermal expansion and cold shrinkage. In Fig. 7(d), high/low SLPA happened in most El Niño events (11 of 15 events)/La Niña events (6 of 11 events), indicating that SLPA may be another factor contributing to the low/high SLAs in the PRE during ENSO. In Fig. 7(e), it can be seen that ENSO had strong impacts on ZWA. There are 13 of 15 El Niño events with strong positive ZWA and 10 of 11 La Niña events

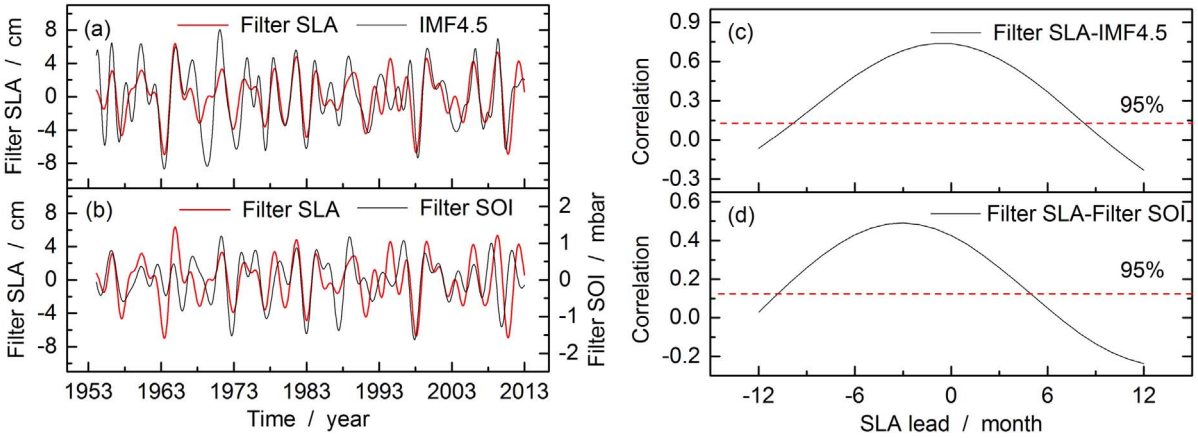

Fig. 6. Variations of filter SLA with intrinsic mode function 4.5 (IMF4.5) (a) and filter Southern Oscillation Index (SOI) (b) and corresponding cross-correlations of filter SLA and IMF4.5 (c) and filter SLA and filter SOI (d).

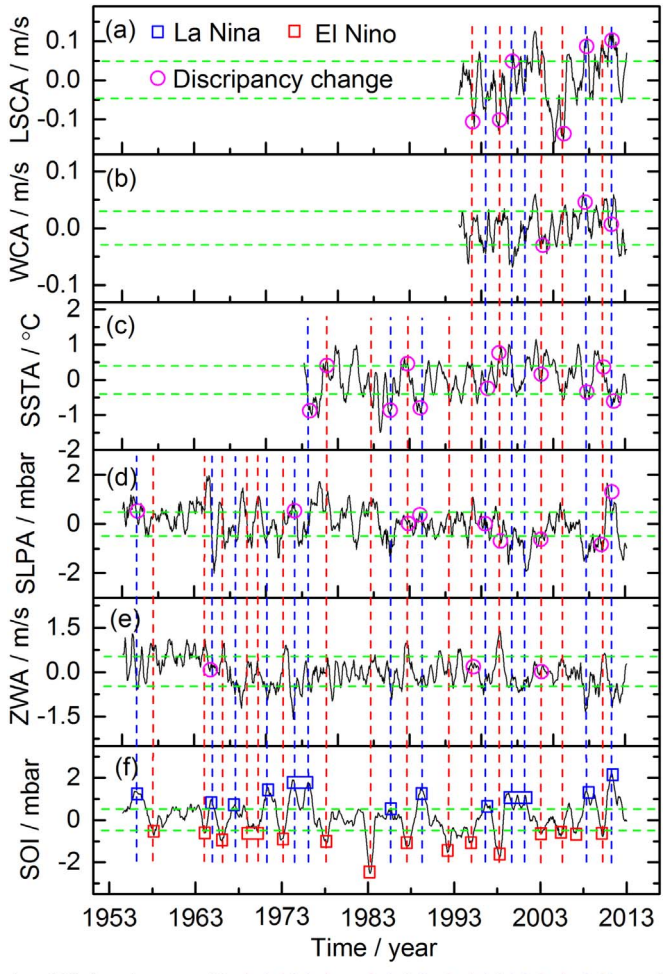

Fig. 7. Variations of seven-month moving average Luzon strait current anomalies (LSCA) (a), westward current anomalies (WCA) (b), sea surface temperature anomalies (SSTA) (c), sea level pressure anomalies (SLPA) (d), zonal wind anomalies (ZWA) (e) and Southern Oscillation Index (SOI) (f). Red and blue dashed vertical lines indicate El Niño and La Niña events; green horizontal lines indicate anomalously large fluctuations. (For interpretation of the references to color in this figure legend, the reader is referred to the web version of this article.)

with strong negative ZWA. Negative zonal wind indicated a north wind, under which overall westward Ekman transport would move seawater along the South China coasts to the PRE and further led to the high SLA, and vice versa.

The filter signals of these regional and local factors were obtained using the 2–7 years' band pass filters. Fig. 8 gives the change and correlation results of filter SOI with filter LSCA, WCA, SLPA and ZWA and filter ONI with filter SSTA. In Fig. 8(a), the filter ZWA showed reverse changes with filter SOI over 1954–2012 and positive/negative ZWA occurred in almost all El Niño/La Niña events. In Fig. 8(b), there were high/low filter SLPA in most El Niño/La Niña events over 1954–2012. From Fig. 8(c), the SSTA showed change similar to ONI in most years of 1975–2012 and high/low filter SSTA happened in most El Niño/La Niña events. No regular changes of filter LSCA and filter SOI can be found because either similar or reverse changes of LSCA and SOI happened over 1993–2012 (Fig. 8d). In Fig. 8(e), filter WCA showed reverse changes with filter SOI and positive/negative WCA happened in most El Niño/La Niña events, indicating that there was less/more seawater transport into the PRE in most El Niño/La Niña events.

Sequence of these factors based on their correlations with filter SOI or ONI from the highest to the lowest was below: ZWA, WCA, SSTA, SLPA and LSCA and the corresponding correlations were −0.79, −0.52, 0.42, −0.27 and 0.19, respectively. If ENSO event was the reason for these factors' anomalies, the lead time response of these factors relative to SOI or ONI would not happen. All factors, except SSTA, had lag time responses with filter ONI for their maximum correlations. The response time lags of filter ZWA, WCA, SLPA and LSCA with filter SOI were 2-month, 4-month, 2-month and 4-month, respectively. The maximum correlation between filter SSTA and filter ONI was above 0.40, but SSTA led ONI by 2 months (Fig. 8h). The low correlation of LSCA and SOI indicates that the effect of ENSO on regional LSCA was weak. The high correlations and response time lags of filter ZWA and WCA with filter SOI reveals that ENSO had significant effects on ZWA and WCA.

The changes and correlations of filter SLA with filter ZWA, SLPA, SSTA, LSCA and WCA were shown in Fig. 9. The positive/negative ZWA (Fig. 9a) and WCA (Fig. 9e) often occurred accompany with the low/high SLA in the PRE, which means that weak/strong north wind and westward current anomalies happened, a weak/strong SLA frequently occurred. That is, ZWA and WCA may have caused the SLAs in the PRE during ENSO. At most cases, low/high SLA occurred when SLPA were strong/weak (Fig. 9b). SSTA and LSCA did not show too much regular changes with SLA (Fig. 9c and d) because when SLAs were anomalously high, there were either high or low values of SSTAs and LSCAs, and vice versa.

The order of these factors based on their correlations with filter SLA from the highest to the lowest was below: WCA, ZWA, SLPA, LSCA, and SSTA and the corresponding correlations were −0.61, −0.46, −0.41, 0.26 and 0.13, respectively. The top two factors were WCA (Fig. 9j) and ZWA (Fig. 9f) and they had maximum correlations with SLAs with no time lag, indicating that WCA and ZWA were two direct factors affecting sea level in the PRE during ENSO. The maximum correlation between filter SLPA and SLA was −0.41 when SLA was lagged 1-month, suggesting that SLPA was another factor affecting SLA in the PRE. Although SLA had 5-month lag of LSCA, their maximum correlation was < 0.30, indicating that LSCA had weak effect on SLA in the PRE. SSTA may not be a factor changing SLA in the PRE during ENSO because SLA led SSTA for 2-month and their correlation was < 0.2.

ZWA and WCA were always the top two factors with high correlations with both SOI and SLA. Whether the ZWA caused the coastal WCA change was also studied. From the changes of ZWA and WCA in Fig. 10(a), they had similar changes at most time. The maximum correlation of ZWA and WCA was 0.51 when WCA had 1-month lag. The change and response time of ZWA and WCA revealed that the westward current outside the PRE had changes lag the north wind anomalies, i.e., WCA may be a result of the ZWA through wind driven current.

The relationship between LSCA and WCA was also studied and they showed the similar change at some time, but sometimes the reverse change happened. Five of 10 ENSO events over 1993–2012 with strong/weak LSCA (Fig. 7a), but WCA showed changes opposite to LSCA (Fig. 7b). The maximum correlation between WCA and LSCA was 0.40 (Fig. 10d), but WCA led LSCA by 8-month (Fig. 10d), The changes and response time between LSCA and WCA revealed that westward current outside the PRE did not change with LSC intrusion, i.e., it was not a result of the LSCA.

3.3. The main factors affecting SLA

According to the correlation and response time results, ZWA and WCA were two key factors related to SOI and SLA. The possible mechanism relationship among SOI, SLA, ZWA and WCA were given in Fig. 11 based on their correlations and response time. It can be seen that SLA in the PRE had the maximum correlation with SOI after a 3-month lag of SLA (SOI → SLA), suggesting that a response time of SLA to SOI was 3 months. The overall response time lags of SLA and SOI through the indirect processes of ZWA and WCA, i.e., SOI → ZWA → WCA → SLA, were also 3 months and the absolute values of correlations between each factor were all above 0.50. The process interpretation was follows: the occurrence of ENSO event will bring trade wind anomalies

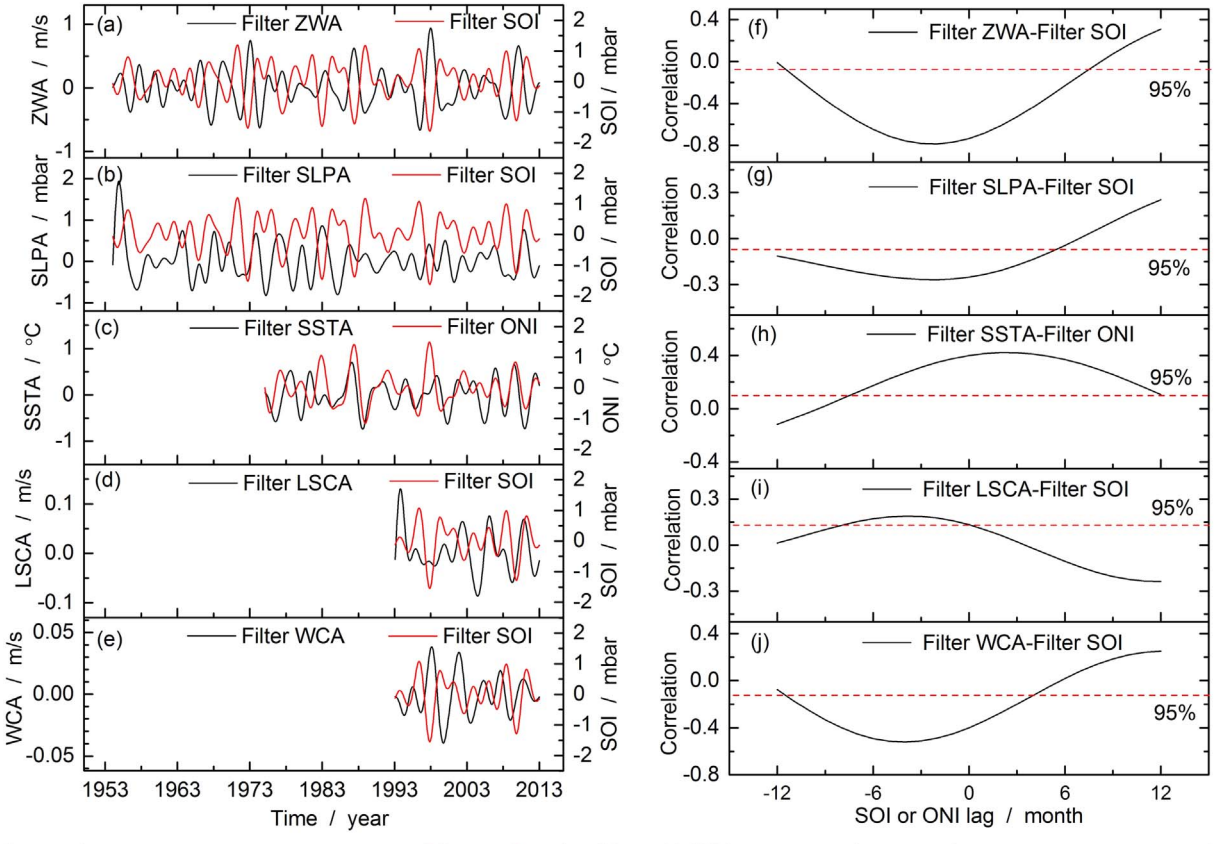

Fig. 8. Variations of filter Southern Oscillation Index (SOI) with filter zonal wind anomalies (ZWA) (a), filter sea level pressure anomalies (SLPA) (b), filter sea surface temperature anomalies (SSTA) (c), filter Luzon strait current anomalies (LSCA) (d) and filter westward current anomalies (WCA) (e) and corresponding cross-correlations of filter SOI with filter ZWA (f), filter SLPA (g), filter SSTA (h), filter LSCA (i) and filter WCA (j).

in the equatorial regions, as a result of which, there are obviously positive/negative ZWAs in the PRE during most El Niño/La Niña events. Then, under the action of wind driven current, the positive/negative zonal wind anomalies brought the weak/strong coastal westward current anomalies. Finally, the low/high SLAs in the PRE occurred in most El Niño/La Niña events after less/more seawater were transported into PRE through Ekman transport.

3.4. Typical ENSO events and regional SLA change

We first analyzed the HYCOM daily mean SSH ~65 km from coastlines (~21.33°N and 114.08°E) and local SSH from the Quarry Bay station in 2010 and 2011 (Fig. 12a and b). Trends of open sea SSHs agreed well with coastal ones after reference datum correction, and their correlations were 0.92 and 0.86. This demonstrates that the HYCOM simulation results are credible and local sea level could effectively indicate regional sea level changes.

Compared with the El Niño neutral situation, weak/strong SLAs were found in the El Niño/La Niña periods (Fig. 12c and d), effectively validating the results of our statistical analysis showing that low/high sea levels were frequent in El Niño/La Niña events. It was also found that anomalous sea level changes not only occurred in the PRE but also in South China coastal waters. From the SSTA variations in the El Niño/La Niña periods (Fig. 12e and f), strong/weak SSTAs occurred over most of the South China coastal water, suggesting that ocean temperature there was important in modulating the falling/rising sea level in El Niño/La Niña events and the result was similar with that in Fig. 7(c). For SLPA (Fig. 12g and h), instead of the strong/weak SLPA in most El Niño/La Niña events (Fig. 7d), the opposite situation was discovered. This is because SLPAs in the selected El Niño and La Niña events were from one of four strong El Niño events with weak SLPAs and one of five La Niña events with strong SLPAs (Fig. 7d). These anomalously weak/strong SLPAs could lead to the strong/weak SLAs, which suggested that other factors such as wind-driven current may cause the anomalously weak/strong SLA during El Niño/La Niña events. For current anomalies (Fig. 12i and j), current flow direction anomalies in the El Niño and La Niña periods were eastward and westward, respectively. The strong westward current would generate water convergence after blockage by Hainan Island and possibly a strong SLA, and vice versa for eastward current.

From the current anomalies (Fig. 12i and j) and actual ocean current in the studied El Niño, La Niña and El Niño-neutral periods (Fig. 13a–c), the current in the South China coastal waters was always westward, but it became weaker/stronger in El Niño/La Niña periods than those in the El Niño-neutral situation, and eventually led to the relatively low/high SSHs (Fig. 13a and b). Therefore, coastal ocean current should be a dominant factor leading to the anomalous sea level changes in ENSO, which verified the results in Figs. 8(e), 9(e) and 11. It was also found that the coastal current was not from the Kuroshio intrusion, which mainly flowed into the interior SCS or along the edge of the continental shelf (Fig. 13a and b). According to the wind driven current and Ekman transport theory, the meridional currents were related to zonal wind stress. Wind stresses are depicted in Fig. 12d–f, from which it is seen that all wind stresses in the study areas were negative and southward. Such southward wind stress would drive the westward current in the South China coastal waters. These southward wind stresses and westward currents, in sequential order, became stronger in the El Niño, El Niño-neutral, and La Niña periods, indicating that the zonal (north) winds were definitely the dominant factor producing the coastal westward current anomalies, which also well verified the conclusion in Fig. 11.

We quantitatively analyzed seawater transport driven by zonal wind

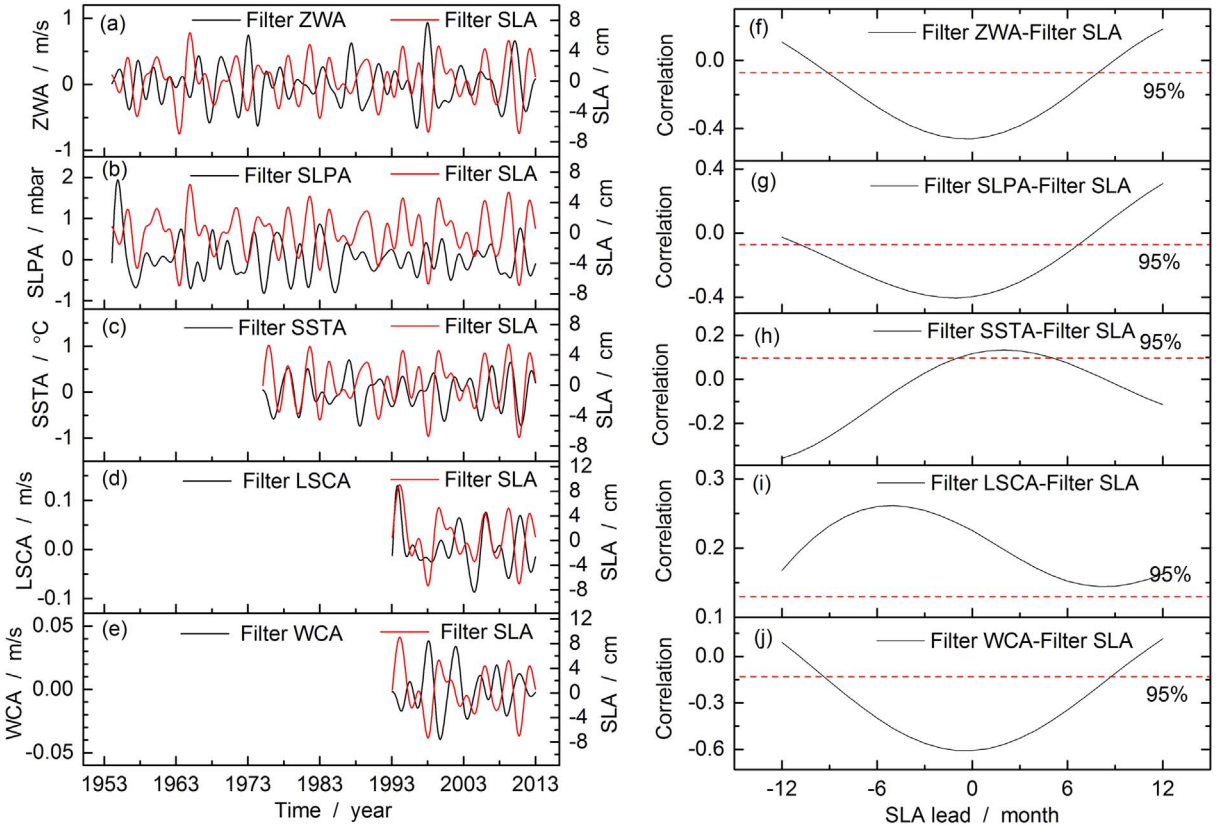

Fig. 9. Variations of filter Sea level anomalies (SLA) with filter zonal wind anomalies (ZWA) (a), filter sea level pressure anomalies (SLPA) (b), filter sea surface temperature anomalies (SSTA) (c), filter Luzon strait current anomalies (LSCA) (d) and filter westward current anomalies (WCA) (e) and corresponding cross-correlations of filter SLA with filter ZWA (f), filter SLPA (g), filter SSTA (h), filter LSCA (i) and filter WCA (j).

for above three typical periods of El Niño (January 2010), La Niña (January 2011), and ENSO-neutral event (January 2013). A cross section AA′ (Fig. 13a) at 115°E and 20.94°–22.5°N was selected to analyze seawater volume transport variation caused by wind-driven current. Maximum and mean depths along this cross section are 150 and ~84 m, and distance from the offshore site (115°E and 22.5°N) and coastline is ~160 km. From previous study, the coastal current is mainly driven by wind (Wang et al., 2017). At the cross section, the seawater volume transport calculated from the east–west current velocity decreased by 21.07% in the El Niño event and increased by 44.03% in the La Niña event as compared to the ENSO-neutral situation. Intrusion seawater accumulates because of blockage by Hainan Island. The small/large amount of westward water transport forced by weak/strong north winds during El Niño/La Nina ultimately led to the divergence/convergence of seawater in the PRE region and further low/high SLAs. Based on above regional results, the study of sea level change and related impact factors in the PRE during El Niño and La Niña periods may also be applied to all the South China coastal waters.

4. Discussion

4.1. Mechanism of ENSO effects on SLA in PRE

El Niño and La Niña events reflect large-scale atmosphere pressure

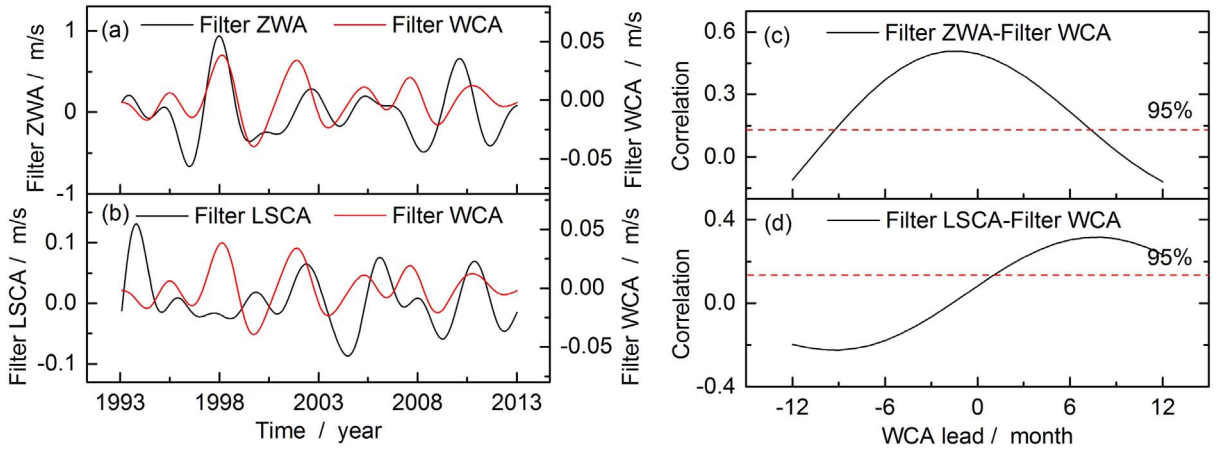

Fig. 10. Variations of filter westward current anomalies (WCA) with filter zonal wind anomalies (ZWA) (a) and filter Luzon strait current anomalies (LSCA) (b) and corresponding cross-correlations of filter WCA with filter ZWA (c) and filter LSCA (d).

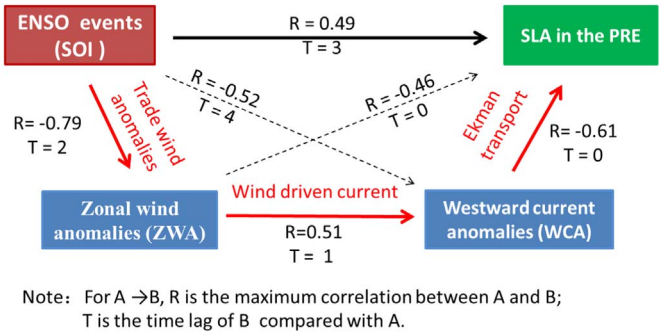

Fig. 11. The mechanism relationship of ENSO and SLA in the PRE through the actions of zonal wind anomalies (ZWA) and coastal westward current anomalies (WCA); The correlations and response time delay among Southern Oscillation Index (SOI), ZWA, WCA and SLA and the related physical processes of trade wind, wind driven current and Ekman transport are shown.

variations between the western and eastern tropical Pacific via the Walker circulation (Webster and Yang, 1992). During El Niño or La Niña phases, atmospheric pressure anomalies in the tropical Pacific modulate the strength of the easterly trade wind in the equatorial Pacific. This produces westward current and other regional climate anomalies, such as the East Asian monsoons and tropical cyclone anomalies in the SCS (R. Huang et al., 2004; Z. Huang et al., 2004; Lee and Cheng, 2011; Zhai and Hu, 2012). The large-scale ocean-atmosphere changes further lead to regional and local oceanic current, sea level pressure, wind and sea surface temperature anomalies, which ultimately have comprehensive impacts on sea level changes in the PRE.

For regional factor of Kuroshio intrusion current, positive correlation of the SOI with LSCA (r = 0.19, 2-month lag of LSCA) suggests that more/less seawater flowed into the SCS through the Luzon Strait during the El Niño/La Niña episodes. These results are consistent with previous studies (Qu et al., 2004; Yang et al., 2014). The maximum correlations of LSCA and SOI and SLA were both < 0.30, suggesting that LSCA was not a key factor affecting SLA in the PRE. Correlation analysis of LSCA and WCA also indicates that this LSCA was not related to the WCA because westward current not only led the LSCA by 8-month but also showed some reverse variations with LSCA during most El Niño/La Niña events (Fig. 7a and b). For Kuroshio intrusion current, inflow seawater through the Luzon strait mainly occurred in winter each year and was less likely to reach the coastal waters above the continental shelf, according to long-term velocity observations from Argos satellite-tracked drifters over 1989–2002 (Luca et al., 2004). Furthermore, the inflow either moved back to the Pacific Ocean or entered the interior SCS mainly along the edge of the continental shelf (Nan et al., 2015; Luca et al., 2004; Liang et al., 2003; Luca et al., 2004). Because of a lack of observation data and the unstable flow state of Kuroshio intrusions, the detailed mechanism needs further investigation.

At local scale, geostrophic velocities in the open sea near the PRE (~20°N, ~114°E) confirm a coastal westward current having strong correlation with local SLA (r = −0.61, no lag). Weak/strong westward current velocities frequently occurred accompany with low/high sea level anomalies in the PRE during most El Niño events (4 of 5 events)/La Niña events (3 of 5 events) over 1993–2012 (Fig.7b). According to the correlation analysis of ZWA and WCA (r = 0.51, 1-month lag of WCA) and the HYCOM modeling results, it is highly likely that this westward current originates from the zonal wind through wind-driven current process (Fig. 13). For ZWA, it showed opposite temporal variations with SOI, especially during ENSO events (Fig. 7e and f). Of 26 ENSO events (Fig. 7e and f), 13 of 15 El Niño events had large positive ZWAs (ZWA > 0.5 m/s), and 10 of 11 La Niña events had large negative ones (ZWA < −0.5 m/s). The maximum correlation between filter ZWA and filter SOI was −0.79 with 2-month lag of ZWA (Fig. 10f), indicating that ENSO could cause the anomalous change of zonal wind, (i.e., north wind). Studies have shown that ENSO may generate strength and circulation anomalies of the East Asian summer and winter monsoons (R. Huang et al., 2004; Z. Huang et al., 2004), which could explain the PRE wind anomalies during most El Niño/La Niña events. Therefore, zonal wind and its driven westward current were two predominant factors affecting low/high SLAs over the South China coastal waters through the anomalously less/more seawater transport into the PRE from the weak/strong north wind and the following seawater divergence/convergence in El Niño/La Niña events.

SLPA may be another local factor affecting the low/high SLA in the PRE during ENSO. For most cases (Fig. 7d), the high/low SLPA happened in El Niño events (11 of 15 events)/La Niña events (6 of 11 events). However, the overall effect of ENSO on local SLPA was weak because the maximum correlation of filter SOI and SLPA was < 0.30, (r = −0.27, 2-month lag of SLPA, Fig. 8b). The SLPA may be further related to regional tropical cyclone and monsoon anomalies. One study (Lee and Cheng, 2011) indicated a late start of the tropical cyclone season during El Niño years, and more tropical cyclones traversing within 500 km of the Hong Kong region during La Niña years. Thus, anomalously high/low air pressure in the PRE may occur with the presence of tropical cyclones during El Niño/La Niña events. Furthermore, ENSO may affect sea level maxima by modulating the number of tropical cyclones reaching China's coasts (Feng and Tsimplis, 2014). The correlation of SLPA and SLA was −0.41 when SLA lagged by 1-month, indicating that high/low SLPA (Fig. 9b and g) often led to the weak/strong SLA. The occurrence frequencies of high/low SLPAs in El Niño/La Niña events over 1954–2012 were lower than those of strong/weak ZWA (Fig. 7d and e) and the correlations of SLPA with SOI and SLA (Figs. 8g and 9g) were also lower than those of ZWA (Figs. 8f and 9f), which suggests that SLPA may be a secondary factor affecting SLA in the PRE during ENSO.

For local SSTA, the maximum correlation between filter SSTA and ONI was 0.42 (Fig. 8c and d), but SSTA led ONI by 2 months. The maximum correlation between SSTA and SLA was ~0.13 when SLA had a 2-month lead relative to SSTA (Fig. 9c and d). The unreasonable response time suggests that ENSO did not directly affect local SSTA in the PRE. The Ekman transport of cold and warm seawater in the coastal region through the anomalous wind in ENSO may produce the SST anomalies. Lee and Cheng (2011) found that spring and winter rainfall in the Hong Kong region increased during El Niño events. Therefore, the anomalous wind and precipitation may affect SSTAs and induce the atypical response times of SSTA to ONI and SLA (Fig. 10d and f). In most El Niño (6 of 10 events)/La Niña events (6 of 7 events), high/low SSTAs occurred simultaneously with low/high SLA, suggesting that SSTAs played the role in modulating the falling/rising of SLAs during most El Niño/La Niña events. Overall, the impact of SSTA on local SLAs was weaker than those of ZWA and WCA from the correlations. This explains the weak/strong SLAs during El Niño/La Niña events, even if high/low SSTAs occurred.

The possible mechanism of ENSO effects on interannual sea level variability in the PRE is likely a combination of multiple factors. ZWA and coastal WCA are two dominant effects on SLA and SLPA is a secondary factor. Less/more seawater transport into the PRE via an anomalously weak/strong westward current driven by weak/strong north wind together with an anomalously strong/weak SLPA in most cases led to the low/high sea levels in the PRE during most El Niño/La Niña events. In contrast, SSTA caused by other multiple processes such as large scale global warming, local rainfall, and regional wind-driven seawater Ekman transport can suppress local sea level falling/rising during El Niño/La Niña events. The Kuroshio intrusion current may be an influential factor but not an important one. For these factors, wind driven current, that is the regional coastal upwelling and circulation, is much important for sea level changes in the South China coastal waters rather than in the PRE region during the ENSO events.

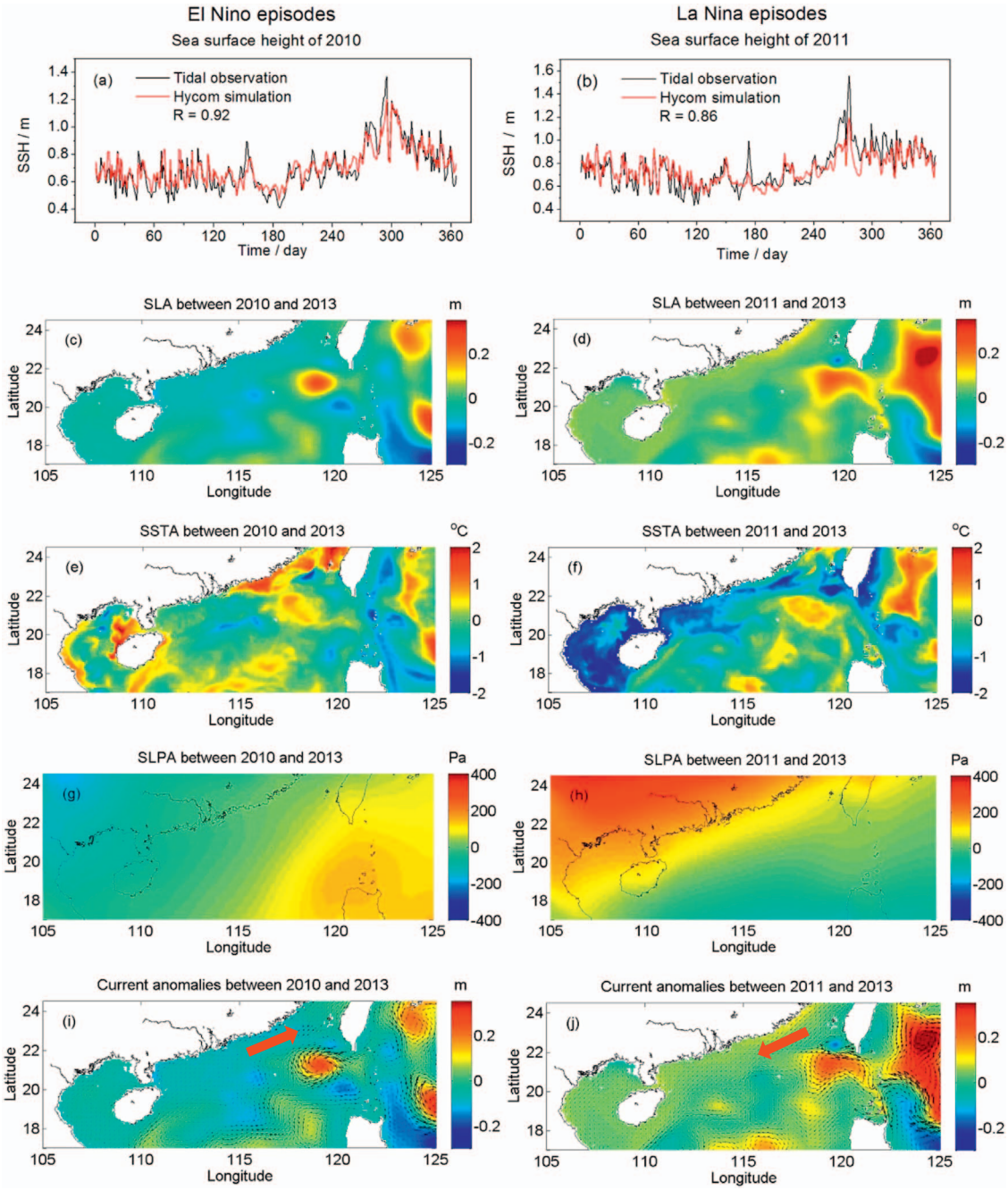

Fig. 12. Comparison of El Niño and La Niña situations using sea surface height from tidal observations and HYCOM simulations for 2010 and 2011 (a) and (b) respectively; January mean SLA (c) and (d); January mean sea surface temperature anomalies (SSTAs) (e) and (f), January mean sea level pressure anomalies (SLPAs) (g) and (h), January mean current anomalies (i) and (j).

4.2. Implications of future ENSO in the PRE

A new El Niño episode has intensified in the tropical Pacific beginning in 2015 (NOAA Climate Prediction Center; http://www.cpc.ncep.noaa.gov/). According to the quantitative effect of ENSO on SLA in the PRE, the sea level fluctuated from −8.70 to 8.11 cm. Therefore, the sea level in the PRE region during the present El Niño episode could decline as much as 8.70 cm compared with El Niño-neutral years. This result was verified by the 2015 annual mean sea level in Hong Kong waters, which declined ~4 cm compared with the previous year (HKO website reports; http://gb.weather.gov.hk).

Precipitation in South China is strongly correlated with ENSO, with much more in El Niño events and less in La Niña events (Xu et al., 2007). Anomalously heavy precipitation integrating water level and wave can cause floodwaters. Studies of flood frequency in the Pearl River basin have indicated more flood events and risk in the northeast portion because of intensifying precipitation (Q. Zhang et al., 2015; R. Zhang et al., 2015). The Pearl River, China's third largest river in discharge, has uneven flow and 80% of its discharge occurs during flood season (Zhang et al., 2010; Q. Zhang et al., 2015; R. Zhang et al., 2015). Moreover, the South China coast is one of the world's areas most vulnerable to typhoons, especially during La Niña events (Chan et al., 2004; Lee and Cheng, 2011). Studies have shown that rising SST has had direct links to the frequencies and intensities of tropical cyclones over the last 30 years (Hoyos et al., 2006; Zheng and Tang, 2007). Once heavy precipitation and more frequent tropical cyclones occur during El

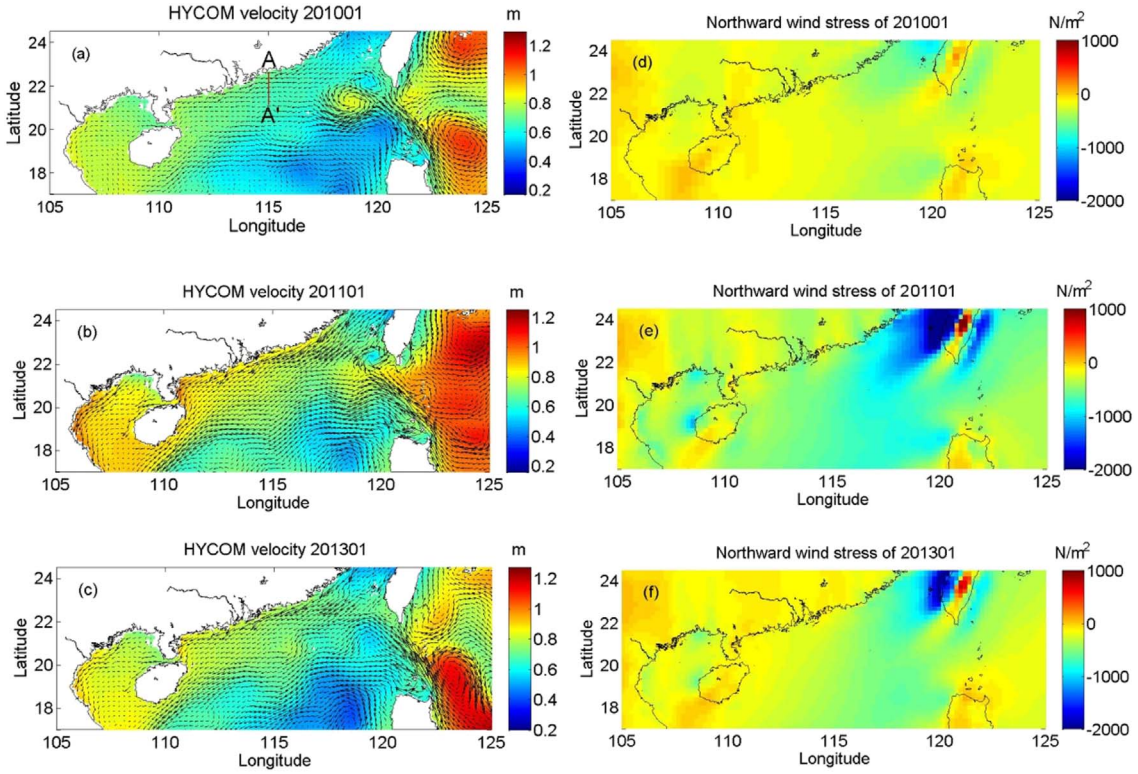

Fig. 13. Monthly mean ocean current (velocity vectors) and sea level height (contours) for January 2010 (a), 2011 (b) and 2013 (c), and corresponding monthly mean northward wind stress for January 2010 (d), 2011 (e) and 2013 (f).

Niño or La Niña events, massive flooding, seawater intrusion, and land inundation will cause severe property damage and casualties in the prosperous and densely populated PRE region. These phenomena were similar to those in the Yangtze River flood of 1997–1998, which occurred during a strong El Niño event (Lau and Weng, 2001). The present research into the mechanism of ENSO and its impacts on sea level change in the PRE can provide insight for future disaster prevention. The monitoring of regional zonal wind and coastal current strength can offer risk prediction of land inundation and seawater intrusion because the weak/strong SLA is strongly affected by the weak/strong wind-driven current in ENSO. Once the extreme ENSO event is identified in the tropical Pacific Ocean, 3-month lag of local SLA in PRE relative to ENSO will provide sufficient warning time. Therefore, it is helpful for Oceanic Administration in Guangdong province to make coastal hazard mitigation planning 3 months ahead according to the regional wind-driven current during ENSO.

5. Conclusions

Local sea level changes in the PRE region showed a downward trend before the 1990s, and then increased with fluctuation. Low/high sea levels were frequent in El Niño/La Niña years. Over the past 59 years, there were three SLA maxima during strong La Niña events, and four minima in strong El Niño events.

Interannual sea level change in the PRE was related to ENSO. For sea level variability in the PRE, ~3 and ~5 years' cycle was related to ENSO. The corresponding sea level signal named IMF4.5 with period of ~3 and ~5 year and fluctuation of −8.70–8.11 cm was identified, and the maximum correlation between it and the SOI was ~0.38, greater than the regional correlation levels of 0.05–0.3. Another sea level signal named filter SLA with fluctuation of −6.96–6.38 cm was extracted using 2–7 years' band pass filter method. This signal showed changes similar to IMF4.5 (r = 0.79, no time lag) and had the maximum correlation with filter SOI of 0.49. Both the two signals showed that tropical ENSO events took ~3 months to affect sea level in the PRE over 1954–2012, causing local sea level to fluctuate within 10 cm.

ENSO events affect sea level in the PRE through multiple processes. Weak/strong SLAs in the PRE are dominated by less/more seawater transport into the PRE, driven by anomalously weak/strong north winds during El Niño/La Niña events. Anomalously high/low air pressure also led to weak/strong SLAs in most El Niño/La Niña events. In contrast, anomalously high/low sea surface temperature modulated falling/rising SLA during most El Niño/La Niña events, but its impact was relatively weak. The regional Kuroshio intrusion current might affect local SLA, but was not major. Related mechanisms can be extended to the South China coastal waters.

The regional wind-driven seawater transport mechanism was verified using HYCOM simulation. Coastal seawater volume transport along a ~160 km wide cross section near the PRE to decrease by 21.07% in a typical El Niño period (January 2010) and increase by 44.03% in a typical La Niña period (January 2011) compared to an ENSO neutral situation (January 2013). The ~5-year ENSO periodicity was validated by a strong El Niño event during 2015–2016. Annual mean sea level in the studied water in 2015 declined ~4 cm compared with the previous year, verifying the decline of 8.70 cm in El Niño events. This research has potential applications for disaster prevention during extreme El Niño or La Niña events. The regional wind monitoring can offer risk prediction of land inundation and seawater intrusion because the SLA is strongly affected by the wind-driven seawater transport in ENSO. Three-month lag of SLA in PRE relative to the tropical ENSO event will provide sufficient warning time.

Acknowledgments

This work was supported by the National Basic Research Program of China (No. 2014CB745002) and Shenzhen Science and Technology Plan Project of China (JCYJ20150831192329178 and JCYJ20160608165926763). We express our gratitude to the Hong Kong

Observatory, Government of the Hong Kong Special Administrative Region, China, for providing the tide and sea surface temperature data. Thanks also go to the National Centers for Environmental Prediction/National Center for Atmospheric Research (NCEP/NCAR) (http://www.cpc.ncep.noaa.gov/) and the Climate Prediction Center of NOAA for providing the monthly data of SLP, SST, SOI, ONI and wind (http://www.esrl.noaa.gov/psd). We also thank AVISO for providing free data of SLA and absolute geographic velocity (http://www.aviso.altimetry.fr/), and acknowledge the Hybrid Coordinate Ocean Model (HYCOM) for analysis and reanalysis data of SSH, SST, eastward and northward sea water velocity, surface downward northward stress (http://tds.hycom.org/). Finally, the European Center for Medium-Range Weather Forecasts (ECMWF) furnished monthly mean sea level pressure (http://apps.ecmwf.int/datasets/).

References

Bi, H., Peterson, W.T., Strub, P.T., 2011. Transport and coastal zooplankton communities in the northern California current system. Geophys. Res. Lett. 38, L12607.
Cazenave, A., Nerem, R.S., 2004. Present-day sea level change: observations and causes. Rev. Geophys. 42, RG3001.
Cazenave, A., Henry, O., Munier, S., Delcroix, T., Gordon, A.L., Meyssignac, B., Llovel, W., Palanisamy, H., Becker, M., 2012. Estimating ENSO influence on the global mean sea level over 1993–2010. Mar. Geod. 35, 82–97.
Cazenave, A., Dieng, H.B., Meyssignac, B., Schuckmann, K.V., Decharme, B., Berthier, E., 2014. The rate of sea-level rise. Nat. Clim. Chang. 4, 358–361.
Chan, J.C.L., Liu, K.S., Ching, S.E., Lai, E.S.T., 2004. Asymmetric distribution of convection associated with tropical cyclones making landfall along the South China Coast. Mon. Weather Rev. 132, 2410–2420.
Chang, C.W.J., Hsu, H.H., Wu, C.R., Sheu, W.J., 2008. Interannual mode of sea level in the South China Sea and the roles of El Niño and El Niño modoki. Geophys. Res. Lett. 35, L03601.
Chang, Y., Du, L., Zhang, S., 2013. Sea level variations in the tropical Pacific Ocean during two types of recent El Nino events. Glob. Planet. Chang. 108, 119–127.
Chen, J., Wen, Z., Wu, R., Chen, Z., Zhao, P., 2014. Interdecadal changes in the relationship between Southern China winter-spring precipitation and ENSO. Clim. Dyn. 43, 1327–1338.
Cheng, X., Qi, Y., 2007. Trends of sea level variations in the South China Sea from merged altimetry data. Glob. Planet. Chang. 57, 3–4.
Cheng, X., Qi, Y., Zhou, W., 2008. Trend of sea level variations in the indo-Pacific warm pool. Glob. Planet. Chang. 63, 57–66.
Cheng, X., Xie, S.P., Du, Y., Wang, J., Chen, X., Wang, J., 2016. Interannual-to decadal variability and trends of sea level in the South China Sea. Clim. Dyn. 46, 3113–3126.
Chowdhury, M.R., Barnston, A.G., Guard, C.C., 2010. Sea-level variability and change in the US-affiliated Pacific island: understanding the high sea levels during 2006–2008. Weather 65, 263–268.
Church, J.A., White, N.J., 2011. Sea-level rise from the late 19th to the early 21st century. Surv. Geophys. 32, 585–602.
Ding, X.L., Chao, J., Zheng, D.W., Chen, Y., 2001a. Long-term sea-level changes in Hong Kong from tide-gauge records. J. Coast. Res. 17, 749–754.
Ding, X., Zheng, D., Chen, Y., Zhao, J., Li, Z., 2001b. Sea level changes in Hong Kong from tide gauge measurements of 1954–1999. J. Geodesy 74, 683–689.
Fang, G., Chen, H., Wei, Z., 2006. Trends and interannual variability of the South China Sea surface winds, surface height, and surface temperature in the recent decade. J. Geophys. Res. 111, 496–511.
Fasullo, J.T., Boening, C., Landerer, F.W., Nerem, R.S., 2013. Australia's unique influence on global sea level in 2010–2011. Geophys. Res. Lett. 40, 4368–4373.
Feng, X., Tsimplis, M.N., 2014. Sea level extremes at the coasts of China. J. Geophys. Res. Oceans 119, 1593–1608.
Han, G., Huang, W., 2009. Low-frequency sea-level variability in the South China Sea and its relationship with ENSO. Theor. Appl. Climatol. 97, 41–52.
Hoyos, C.D., Agudelo, P.A., Webster, P.J., Curry, J.A., 2006. Deconvolution of the factors contributing to the increase in global hurricane intensity. Science 312, 94–97.
Huang, N.E., Wu, M.L., Qu, W., Long, S.R., Shen, S.S.P., Zhang, J.E., 2003. Applications of Hilbert-Huang transform to non-stationary financial time series analysis. Appl. Stoch. Model. Bus. 19, 245–268.
Huang, R., Chen, W., Yang, B., He, R., 2004. Recent advances in studies of the interaction between the East Asian winter and summer monsoons and ENSO cycle. Adv. Atmos. Sci. 21, 407–424.
Huang, Z., Zong, Y., Zhang, W., 2004. Coastal inundation due to sea level rise in the Pearl River delta. China. Nat. Hazards 33, 247–264.
Lau, K.M., Weng, H.Y., 2001. Coherent modes of global SST and sumer rainfall over China: an assessment of the regional impacts of the 1997–98 El Nino. J. Clim. 14, 1294–1308.
Lee, S., Cheng, Y., 2011. An examination of ENSO's effect on the monthly and seasonal climate of Hong Kong from a statistical perspective. ACTA Meteorol. Sin. 25, 34–51.
Li, L., Xu, J.D., Cai, R.S., 2002. Trends of sea level rise in the South China Sea during the 1990s: an altimetry result. Chin. Sci. Bull. 47, 582–585.
Liang, W.D., Tang, T.Y., Yang, Y.J., Ko, M.T., Chuang, W.S., 2003. Upper-ocean currents around Taiwan. Deep-Sea Res. II Top. Stud. Oceanogr. 50, 1085–1105.
Liu, Q., Feng, M., Wang, D., 2011. ENSO-induced interannual variability in the southeastern South China Sea. J. Oceanogr. 67, 127–133.
Liu, B., Wu, G., Ren, R., 2015. Influences of ENSO on the vertical coupling of atmospheric circulation during the onset of South Asian summer monsoon. Cim. Dyn. 45, 1859–1875.
Llovel, W., Becker, M., Cazenave, A., Jevrejeva, B., Alkama, R., Decharme, B., Douvile, H., Ablain, M., Beckley, B., 2011. Terrestrial waters and sea level variations on interannual time scale. Glob. Planet. Chang. 75, 76–82.
Luca, R., Niiler, C.P.P., Lee, D.K., 2004. Observations of inflow of Philippine Sea surface water into the South China Sea through the Luzon Strait. J. Phys. Oceanogr. 34, 113–121.
Nan, Q., Li, T., Chen, J., Nigma, R., Yu, X., Xu, Z., Yang, Z., 2014. Late Holocene (~2 ka) East Asian monsoon variations inferred from river discharge and climate interrelationships in the Pear River Estuary. Quat. Res. 81, 240–250.
Nan, F., Xue, H., Yu, F., 2015. Kuroshio intrusion into the South China Sea: a review. Prog. Oceanogr. 147, 324–333.
Nerem, R.S., Chambers, D.P., Choe, C., Mitchum, G.T., 2010. Estimating mean sea level change from the TOPEX and Jason altimeter missions. Mar. Geod. 33, 435–446.
Peng, D., Palanisamy, H., Cazenave, A., Meyssignac, B., 2013. Interannual sea level variations in the South China Sea over 1950–2009. Mar. Geod. 36, 164–182.
Qu, T.D., Kim, Y.Y., Yaremchuk, M., Tozuka, T., Ishida, A., Yamagata, T., 2004. Can Luzon Strait transport play a role in conveying the impact of ENSO to the south China Sea? J. Climate 17, 3644–3657.
Rahmstorf, S., 2007. A semi-empirical approach to projecting future sea-level rise. Science 315, 368–370.
Rilling, G., Flandrin, P., Goncalves, P., 2003. On Empirical Mode Decomposition and Its Algorithms. IEEE-EURASIP Workshop on Nonlinear Signal Image Process. NSIP-03. Grado Italy.
Rong, Z., Liu, Y., Zong, H., Cheng, Y., 2007. Interannual sea level variability in the South China Sea and its response to ENSO. Glob. Planet. Chang. 55, 257–272.
Shi, X., Chen, T., Yu, K., 2008. Sea-level changes in Zhujiang estuary over last 40 years. Mar. Geol. Quat. Geol. 28, 127–134.
Soumya, M., Vethamony, P., Tkalich, P., 2015. Inter-annual sea level variability in the southern South China Sea. Glob. Planet. Chang. 133, 17–26.
Tseng, Y.H., Breaker, L.C., Chang, E.T.Y., 2010. Sea level variations in the regional seas around Taiwan. J. Oceanogr. 66, 27–39.
Wang, L., Zhang, Q., Li, W., 2012. Diagnosis of the ENSO modulation of tropical cyclogenesis over the southern South China Sea using a genesis potential index. Acta Oceanol. Sin. 31, 54–68.
Wang, L.L., Li, Q., Bi, H.S., Mao, X.Z., 2016. Human impacts and changes in the coastal waters of south China. Sci. Total Environ. 562, 108–114.
Wang, H., Liu, K., Gao, Z., Fan, W., Liu, S., Li, J., 2017. Characteristics and possible causes of the seasonal sea level anomaly along the South China Sea coast. Acta Oceanol. Sin. 36, 9–16.
Webster, P.J., Yang, S., 1992. Monsoon and ENSO: selectively interactive systems. Q. J. R. Meteorol. Soc. 118, 877–926.
Woodworth, P., Menendez, M., 2015. Changes in the mesoscale variability and in extreme sea levels over two decades as observed by satellite altimetry. J. Geophys. Res. Oceans 120, 64–77.
Wu, Z., Milliman, J.D., Zhao, D., Zhou, J.Q., Yao, C.H., 2014. Recent geomorphic change in LingDing Bay, China, in response to economic and urban growth on the Pearl River Delta, Southern China. Glob. Planet. Chang. 123, 1–12.
Xu, Z.X., Li, J.Y., Takeuchi, K., Ishidaira, H., 2007. Long-term trend of precipitation in China and its association with the El Niño-southern oscillation. Hydrol. Process. 21, 61–71.
Yang, L., Xu, D., Xu, M., Sui, D., Wu, P., 2014. A study of correlation between Pacific Decadal Oscillation and El Nino-Southern Oscillation and the strength of Kuroshio intrusion into the South China Sea. Acta Oceanol. Sin. 37, 17–26 (in Chinese with English abstract).
Yin, K.D., Harrison, P.J., Chen, J., Huang, W., Qian, P.Y., 1999. Red tides during spring 1998 in Hong Kong: is El nino responsible? Mar. Ecol. Prog. Ser. 187, 289–294.
Yuan, L.W., Yu, Z.Y., Xie, Z.R., Song, Z.Y., Lu, G.N., 2009. ENSO signals and their spatial-temporal variation characteristics recorded by the sea-level changes in the northwest Pacific margin during 1965–2005. Sci. China Ser. D. 52, 869–882.
Yuan, R., Zhu, J., Wang, B., 2015. Impact of sea-level rise on saltwater intrusion in the Pearl River Estuary. J. Coast. Res. 31, 477–487.
Zhai, F., Hu, D., 2012. Interannual variability of transport and bifurcation of the North Equatorial Current in the tropical North Pacific Ocean. Chin. J. Oceanol. Limnol. 30, 177–185.
Zhang, Y.Z., Ge, E., 2013. Temporal scaling behavior of sea-level change in Hong Kong - multifractal temporally weighted detrended fluctuation analysis. Glob. Planet. Chang. 100, 362–370.
Zhang, S., Mao, X.Z., 2015. Hydrology, sediment circulation and long-term morphological changes in highly urbanized Shenzhen River estuary, China: a combined field experimental and modeling approach. J. Hydrol. 529, 1562–1577.
Zhang, Q., Xu, C.Y., Zhang, Z., Chen, Y.D., 2010. Changes of atmospheric water vapor budget in the Pearl River basin and possible implications for hydrological cycle. Theor. Appl. Climatol. 102, 185–195.
Zhang, Q., Gu, X., Singh, V.P., Xiao, M., Xu, C.Y., 2015. Flood frequency under the influence of trends in the basin, China: changing patterns, causes and implications. Hydrol. Process. 29, 1406–1417.
Zhang, R., Li, T., Wen, M., Liu, L., 2015. Role of intraseasonal oscillation in asymmetric impacts of El Nino and La Niña on the rainfall over southern China in boreal winter. Clim. Dyn. 45, 559–567.
Zheng, G.M., Tang, D.L., 2007. Offshore and nearshore chlorophyll increase induced by typhoon winds and subsequent terrestrial rainwater runoff. Mar. Ecol. Prog. Ser. 333, 61–74.
Zhuang, W., Qiu, B., Du, Y., 2013. Low-frequency western Pacific Ocean sea level and circulation changes due to the conductivity of the Philippine Archipelago. J. Geophys. Res. 118, 6759–6773.